Microscopic double folding potential description of the ^{6}He $+^{12}$C reaction

I. Boztosun,* M. Karakoc, and Y. Kucuk
Department of Physics, Erciyes University, Kayseri, Turkey
(Received 27 March 2008; published 23 June 2008)

We investigate the simultaneous explanation of the ^{6}He + ^{12}C elastic and inelastic scattering and ^{6}He + ^{12}C → ^{4}He + ^{14}C transfer reaction observables at 18.0 MeV within the framework of the coupled-channels Born approximation. In obtaining the microscopic double folding potentials, two different nucleon densities deduced from the no-core shell model and few-body model calculations for the ^{6}He have been used. Although a good agreement between theoretical results and experimental data has been obtained for elastic scattering and transfer reactions data, the theoretical results underestimate the magnitude of the inelastic-2^{+} state data. We present in this article that the deformation of the imaginary part of the optical potential is very important and it overcomes the magnitude problem for the inelastic data for this system.

DOI: 10.1103/PhysRevC.77.064608 PACS number(s): 24.10.Eq, 24.10.Ht, 24.50.+g, 25.60.−t

I. INTRODUCTION

The halo nuclei have become one of the main interests of nuclear physics and nuclear astrophysics since the discovery of their unusual structure [1–12]. During the last two decades, many experiments [1,5,13] have been performed to understand the basic features of the halos and much information has been extracted about the weakly bound nature and the large radial extent in their densities. After these experimental studies, some theoretical models have been suggested to understand the internal structure and the dynamics of their interactions. As a conclusion of all these efforts, many properties of halos have been investigated and a number of neutron or proton rich nuclei have been pronounced in the literature such as ^{6}He, ^{11}Li, ^{11}Be, ^{8}B, ^{13}N, and ^{17}Ne.

The ^{6}He nucleus is the well-known and the most studied halo type nucleus. This nucleus has attracted enormous interest both theoretically and experimentally because of its Borromean structure and the large probability of breakup near the Coulomb barrier [14–16]. It has been argued that ^{6}He is formed from a tightly bound ^{4}He core and loosely attached neutrons, and the ground state structure of ^{6}He has been studied within the frame of various shell models and the few-body model [9,17–22]. The standard shell model has failed to describe essential features of the halo nuclei, although it has a significance in providing spectroscopic information on a number of exotic nuclei. Having noticed the failure, many theorists have improved the standard shell model by using different approaches and they have obtained the ground state properties of the ^{6}He. The no-core shell model (NCSM) conducted by Navratil *et al*. [22] is one of the models used in the description of nuclear structure in recent years. They have carried out a detailed study that shows that the three-nucleon forces play an important role in determining the nuclear properties and they have obtained the physical densities of protons and neutrons for the ^{6}He nucleus by using an *ab initio* approach. In this study, the point-proton and the point-neutron rms radii of ^{6}He have been obtained as 1.763 and 2.361 fm, respectively. Some attempts by using the few-body model have also been carried out in modeling the structure of these nuclei. In these models, it has been assumed that light exotic nuclei such as ^{6}He and ^{11}Li are formed core + valance nucleons and the nuclear matter distributions have been obtained. Al-Khalili and Tostevin [9] have performed the example of the few-body (FB) calculations and have obtained the rms radii for loosely bound two- and three-body systems such as ^{6}He, ^{11}Be, ^{11}Li, and ^{14}Be by considering the corrections to the static density Glauber model calculations of the cross sections. For ^{6}He, they have suggested an rms radius of 2.71 ± 0.04 fm by using the static density S matrix for ^{4}He target scattering.

In addition to these internal structure studies, nuclear reactions induced by ^{6}He at various energies are a popular subject in nuclear physics. Especially, the elastic scattering of ^{6}He with different targets [23–27] has been extensively studied because of the information provided regarding the optical potential as well as the transfer and breakup reactions to investigate the effects of couplings to entrance channels. In recent years, the authors have focused on the ^{6}He + ^{12}C system because of its importance in the stellar synthesis. A lot of experimental studies for this system have been carried out at both low and high energies and the interaction cross sections, momentum distributions, and invariant mass spectra have been measured [23–29]. The analyses of these experimental data have been conducted by using different phenomenological and microscopic models. However, the theoretical analyses have been limited to only some parts of the reaction observables such as cross sections of elastic scattering or inelastic scattering separately.

Milin *et al*. [23] measured the elastic and inelastic scattering of ^{6}He + ^{12}C and also ^{6}He + ^{12}C → α + ^{14}C reactions at 18.0 MeV in the laboratory energy and they have analyzed these data by using the Woods-Saxon shaped phenomenological potentials. They were able to obtain a consistent agreement for the elastic scattering and transfer reaction data, but they were not able to obtain the inelastic-2^{+} data simultaneously with the elastic and transfer channels data. They concluded that a detailed analysis within the framework of the coupled-channels formalism is necessary to explain the experimental data. Matsumoto *et al*. [30] for ^{6}He + ^{12}C and Moro *et al*. [31]

*boztosun@erciyes.edu.tr

for ^{6}He on different target nuclei also conducted a detailed analysis by using the continuum-discretized coupled channels (CDCC) method [32,33]. They obtained excellent agreement with the experimental data for the elastic scattering angular distributions. However, they did not make a prediction for the inelastic-2^+ state data.

Therefore, in this article, within the framework of the coupled-channels approach, we aim to investigate whether or not the microscopic double folding (DF) potential model is an adequate approach for the description of the observables measured by Milin *et al.* [23]. For this purpose, the elastic and inelastic scattering data of ^{6}He + ^{12}C as well as the transfer reaction data of Milin *et al.* [23] have been analyzed by using the DF potential within the framework of the coupled-channels Born approximation (CCBA) [34].

In the next section, we present the theoretical model used in our calculations and the results of these calculations are presented in Sec. III. Section IV is devoted to our summary and conclusion.

II. THEORETICAL CALCULATIONS

To make a simultaneous analysis of the elastic and inelastic scattering of the ^{6}He + ^{12}C system at 18.0 MeV as well as to investigate the coupling effects to entrance channels, we have performed theoretical calculations by using the post representation of CCBA. In CCBA calculations using the code FRESCO [35], two different channels, inelastic channel where target nucleus is in the 2^+ state and transfer channel assuming one-step two-neutron transfer from ^{6}He to ^{12}C, have been added to the elastic channel.

For the elastic and inelastic channels, the real part of the optical potential has been obtained by using the DF potential model. In the folding model, the realistic DF potential can be evaluated by using the nuclear matter distributions for projectile and target nuclei with an effective nucleon-nucleon interaction potential (v_{nn}):

$$V_{DF}(r) = \int\int \rho_P(r_1)\rho_T(r_2)v_{nn}(|\vec{r} + \vec{r}_2 - \vec{r}_1|)d^3r_1 d^3r_2, \quad (1)$$

where ρ_P and ρ_T denote the nuclear matter density of projectile and target nucleus, respectively. To make a comparative study to show the effect of using different ground state density distributions in the folding potential calculations, two different nucleon densities have been used for the projectile. These densities used in our analysis for ^{6}He have been obtained by few-body and no-core shell model calculations taken from the theoretical calculations of Refs. [9] and [22]. The densities of these two models are shown in comparison with each other in Fig. 1 for the projectile ^{6}He. On the other hand, the nuclear matter density for target ^{12}C has been taken to be in the form

$$\rho_P(r_1) = \rho_0\left(1 + wr_1^2\right)\exp\left(-\beta r_1^2\right), \quad (2)$$

where $\rho_0 = 0.1644$ fm^{-3}, $w = 0.4988$ fm^{-2}, and $\beta = 0.3741$ fm^{-2} for target ^{12}C nucleus [36–38].

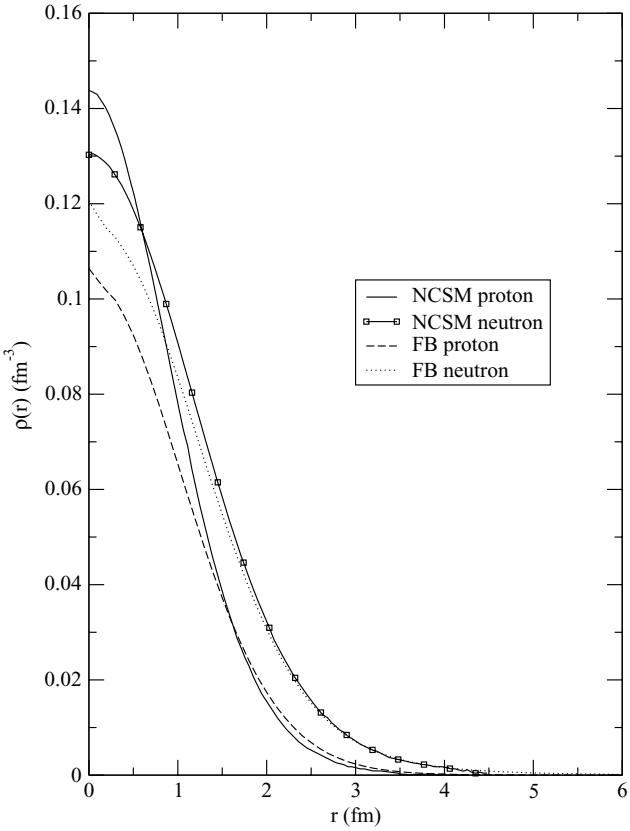

FIG. 1. The proton and neutron density distributions of ^{6}He within NCSM (solid line and solid line with square) and FB (dashed line and dotted line) models.

The M3Y nucleon-nucleon effective interaction has been taken to be in the form

$$v_{nn}(r) = 7999\frac{\exp(-4r)}{4r} - 2134\frac{\exp(-2.5r)}{2.5r} + J_{00}(E)\delta(r)\,\text{MeV}, \quad (3)$$

where $J_{00}(E)$ is varying with the energy as

$$J_{00}(E) = 276[1 - 0.005E/A_p]\,\text{MeV fm}^3. \quad (4)$$

For the transfer channel, the real part of the optical potential has been chosen as the phenomenological Woods-Saxon form

$$V(r) = \frac{-V_0}{(1 + \exp(r - R_V)/a_V)}, \quad (5)$$

where $R_V = r_V(A_P^{1/3} + A_T^{1/3})$. This potential is used for the exit channel (α+^{14}C) and for the core-core potential (α + ^{12}C). The ^{6}He = $\alpha + 2n$ bound state wave function is generated with the potential assuming α and $2n$ clusters in a relative $2S$ state [23,39]. The ^{14}C = ^{12}C + $2n$ binding potential is the same as that in Ref. [40]. The parameters are listed in Table I. CCBA calculation is normalized to the data with the factor $S'_{2n}S_{2n} = 0.45$, where S'_{2n} is the 2n-spectroscopic factor in ^{6}He and S_{2n} is that for the 8.32 MeV state of ^{14}C.

The imaginary potential for all channels has the Woods-Saxon form just like the real part of the transfer channel given by Eq. (5) and the parameters of the imaginary potentials are similar to those in Refs. [23,41,42], except the depth of the

TABLE I. [a]Normalization constants and imaginary potential depth for the present calculations. [b]Varied to give correct separation energy.

Parameters	Nr	V	r_v	a_v	W	r_w	a_w	r_c	Ref.
^{6}He + ^{12}C (NCSM)	1.13[a]				7.0	2.35	0.79	2.3	[42]
^{6}He + ^{12}C (FB)	0.92[a]				7.0	2.35	0.79	2.3	[42]
α + ^{12,14}C		159.0	1.54	0.709	4.15[a]	1.54	0.709	1.2	[41]
^{6}He = $\alpha + 2n$		b	1.7	0.7					[39]
^{14}C = ^{12}C + $2n$		b	1.26	0.6					[40]

imaginary potential for the transfer channel has been reduced to 4.15 MeV.

The real and imaginary potentials are shown in Fig. 2 and their parameters are listed in Table I for the optical potentials of all channels. Furthermore, the comparison of the phenomenological potential and the microscopic potentials for the entrance channel are shown in Fig. 2. For the entrance channel, it is seen that the phenomenological potential used by Milin *et al.* [23] at the interior region is at its deepest around 275.0 MeV and goes to zero faster than the microscopic ones. On the other hand, in the surface region around the strong absorption radius [34] $R_{\rm sar} \simeq 1.5(A_P^{1/3} + A_T^{1/3})$], the phenomenological potential and microscopic potentials have similar values. Nevertheless, the exit channel real potential has a different shape from the other real potentials and it goes to zero very slowly if we compare it with the others.

In the coupled-channels calculations, we assume that the target nucleus ^{12}C has a static quadrupole deformation that can be taken into account by deforming the real part of the potential in the following way,

$$R(\theta, \phi) = r_0 A_p^{1/3} + r_0 A_t^{1/3}[1 + \beta_2 Y_{20}(\theta, \phi)], \qquad (6)$$

where p and t refer to projectile and target nuclei, respectively, and β_2 is the deformation parameter of ^{12}C. We shall use the value of β_2 as -0.6. For the Coulomb deformation, we assume $\beta_2^C = \beta_2^N$.

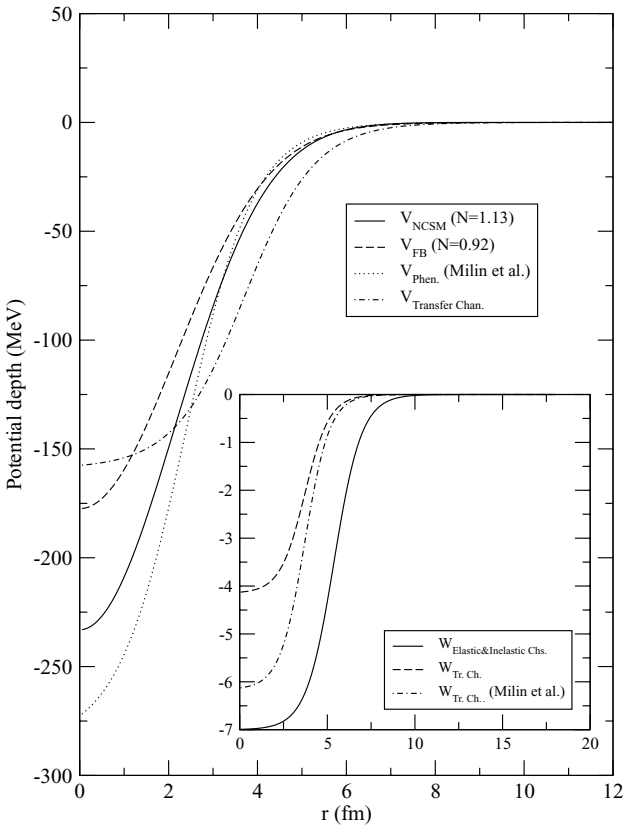

FIG. 2. The shape of the real and imaginary potentials. The solid line shows the potentials obtained by using NCSM, the dashed line shows the potentials obtained by using FB, the dotted line shows the WS potential of Milin *et al.* [23], and the dot-dashed line shows the potential for the transfer channel.

III. RESULTS AND DISCUSSION

The ^{6}He + ^{12}C system has been analyzed in the laboratory system at 18.0 MeV by using both phenomenological and microscopic potentials within the above-described theoretical calculations for a simultaneous explanation of the observables of all reaction channels.

First, we have used the parameters of the study in Ref. [23]. This study has been performed in the framework of the finite range distorted wave Born approximation (FRDWBA) by Milin *et al.* [23]. However, the inelastic channel has not been added in these calculations. Therefore, we have taken into account this channel in our CCBA calculations by using the same parameters [23]. We have obtained good results for the elastic and the transfer channel angular distributions. Nevertheless, the parameters are not adequate for the inelastic-2^+ channel. There is a large difference between the amplitudes of the theoretical and the experimental results as is presented in Fig. 3. The change of the parameters of the real and imaginary potentials does not solve the magnitude problem observed in Fig. 3 between the experimental data and the theoretical results for the inelastic-2^+ state.

After that, our methodology is based on a microscopic DF potential analysis on the elastic channel, because the main contribution to the reaction observables comes from it, then we have added the other channels to the reaction mechanism. To perform this analysis, we have used the target ^{12}C nuclear density as in Refs. [36–38] that is used in the literature commonly. For the projectile ^{6}He, the NCSM [22] and FB model [9] densities have been used to get rid of any unknown discrepancy between the models. Therefore, we have obtained two different potential families for the real part of the optical

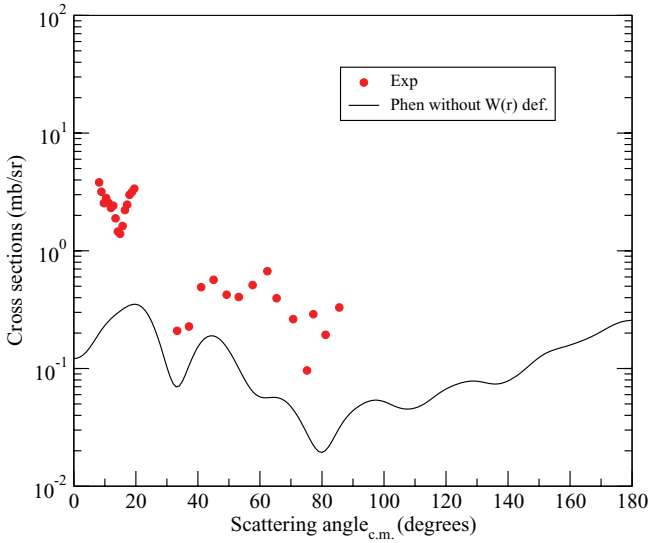

FIG. 3. (Color online) The prediction of the phenomenological WS potential for the inelastic-2^+ state data. See text for the details.

potentials as seen in Fig. 2. The normalization parameters of these potentials have been searched using a χ^2 search code SFRESCO [35]. As a result of these searches, the normalization parameters for the potential have been found to be 1.13 for NCSM and 0.92 for FB.

By using these two microscopic potentials, similar to the phenomenological calculations of Milin *et al.* [23], we have obtained a good description of the elastic and transfer channels data. The individual angular distributions of the elastic channel, shown in the upper part of Fig. 4, are in very good agreement with the experimental data. The magnitude of the cross section is correctly predicted and the minima and maxima are at the correct places with the phases. Both theoretical results are almost the same; the only difference exists around 85° where the NCSM prediction does not have a deep minimum while the FB prediction does. For the transfer channel, the results shown in the bottom part of Fig. 4 are also reasonable: The magnitude of the cross section is correctly predicted. However, although the inelastic-2^+ channel results obtained by using both NCSM and FB potentials are better than the phenomenological results shown in Fig. 3, there still exists a magnitude problem between theoretical predictions and experimental data for this channel. Varying the normalization factors and the parameters of the imaginary potential do not solve this magnitude problem. A simultaneous fit of the elastic, inelastic-2^+, and transfer channels data cannot be achieved by using these microscopic double folding potentials.

The Coulomb excitation by deforming the Coulomb potential in our calculations has not solved this magnitude problem either. The Coulomb excitation has been effective only at forward angles between 0° and 20° for the inelastic angular distribution; however, in the rest of the angular range the theoretical results are the same whether Coulomb excitation is included or not.

This problem is solved by deforming the imaginary potential. It is known that the deformation of the imaginary potential can be useful for the inelastic angular distributions

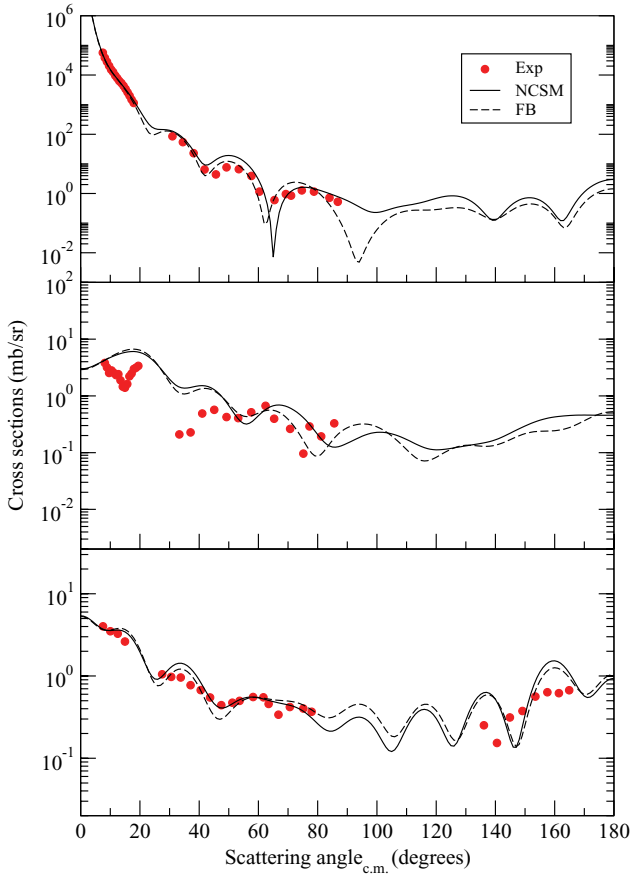

FIG. 4. (Color online) Microscopic DF potential results of the CCBA for the elastic (upper), inelastic-2^+ state (middle), and transfer channel obtained by using the densities of NCSM and FB models for ^{6}He projectile.

only if the real and imaginary parts of the potentials have different radial shapes [34]. Therefore, we have included the deformation of the imaginary potential to our calculations, and then the magnitude problem of the inelastic angular distribution between theoretical and experimental results has been solved as is shown in the middle frame of Fig. 4. Thus, a simultaneous fit of experimental data for the elastic, inelastic-2^+, and transfer channels has been obtained by deforming the imaginary potential along with the real one.

The reaction cross sections of this system have been obtained as 1511 and 1471 mb, respectively, for FB and NCSM while there is no deformation for the imaginary potential of the entrance channel. The deformation of the imaginary potential has a very small effect, resulting with a minor reduction of the value for the reaction cross sections. Our results are in good agreement within the CDCC calculations of Matsumoto *et al.* [30].

IV. SUMMARY AND CONCLUSION

We have conducted a detailed microscopic potential analysis of the $^6\text{He} + ^{12}\text{C} \rightarrow \alpha + ^{14}\text{C}$ reaction at 18.0 MeV in the laboratory system. Two different microscopic double

folding potentials constructed by using the NCSM and FB densities of ^{6}He have been used to obtain the theoretical cross sections. It has been observed that both densities provide a consistent and an adequate description of the elastic scattering and transfer reaction data with small normalization factors. However, they underestimate the inelastic scattering data. Our attempts to explain the elastic, inelastic, and transfer data simultaneously have failed and the magnitude of the inelastic-2^+ data has remained unsolved. Varying the potential parameters and changing the deformation value of ^{12}C have not solved this problem. These same observations have also been observed for the phenomenological Woods-Saxon type potential calculations such as those of Milin *et al*. [23]. Because previous works [30,31] conducted by using the CDCC method do not evaluate the cross section for the inelastic-2^+ state data, further analysis using the CDCC method is necessary to see whether there exists a magnitude problem as in our calculations for the inelastic-2^+ state data.

To fit the inelastic scattering data, it has been shown in this study that, in the coupled-channels calculations, it is necessary to deform not only the real part of the potential but also the imaginary potential. This has solved the magnitude problem of the inelastic-2^+ data and we have been able to achieve a simultaneous fit of the experimental data for the elastic, inelastic-2^+, and transfer channels.

In addition to showing the importance of the deformation of the imaginary potential, our study reveals that the shape of the potentials in the surface region is important in explaining the reaction observables of such reactions. Both FB and NCSM potentials as well as the deep phenomenological Woods-Saxon potentials, which have similar shapes in the surface region, provide similar results although they have very different depths in the interior region. We have also noticed that the Coulomb deformation is important in the forward angles for the inelastic data but at large angles it is negligible. We finally point out that all dynamic effects arising from the distortion and breakup of ^{6}He have been partly taken into account in the optical potentials and the large radius for the imaginary potentials ($r_w = 2.35$ fm) are relevant to the long-range absorption that describes the scattering of weakly bound nuclei.

ACKNOWLEDGMENTS

We thank Drs. A. M. Moro, A. A. Ibraheem, and M. Milin for providing the experimental data and their useful comments. This project was supported by the Turkish Science and Research Council (TÜBİTAK) with Grants 107T824 and 106T024 and by the Turkish Academy of Sciences (TÜBA-GEBİP).

[1] I. Tanihata *et al*., Phys. Rev. Lett. **55**, 2676 (1985).
[2] I. Tanihata, Prog. Part. Nucl. Phys. **35**, 505 (1995).
[3] I. Tanihata, J. Phys. G: Nucl. Part. Phys. **22**, 157 (1996).
[4] A. M. Sánchez-Benitez *et al*., J. Phys. G: Nucl. Part. Phys. **31**, S1953 (2005).
[5] P. G. Hansen and B. Jonson, Europhys. Lett. **4**, 409 (1987).
[6] P. G. Hansen, A. S. Jensen, and B. Jonson, Annu. Rev. Nucl. Part. Sci. **45**, 505 (1995).
[7] K. Riisager, Rev. Mod. Phys. **66**, 1105 (1994).
[8] B. Johnson and K. Riisager, Philos. Trans. R. Soc. London A **356**, 2063 (1998).
[9] J. S. Al-Khalili and J. A. Tostevin, Phys. Rev. Lett. **76**, 3903 (1996).
[10] G. Baur, K. Hencken, D. Trautmann, S. Typel, and H. H. Wolter, Prog. Part. Nucl. Phys. **46**, 99 (2001).
[11] N. A. Orr, Nucl. Phys. **A616**, 155c. (1997).
[12] I. J. Thompson and Y. Suzuki, Nucl. Phys. **A693**, 424 (2001).
[13] I. Tanihata *et al*., Phys. Lett. **B160**, 380 (1985).
[14] G. R. Satchler, Direct Nuclear Reactions (Oxford University Press, 1983).
[15] J. S. Al-Khalili *et al*., Phys. Lett. **B378**, 45 (1996).
[16] R. J. Smith *et al*., Phys. Rev. C **43**, 761 (1991).
[17] J. S. Al-Khalili, J. A. Tostevin, and I. J. Thompson, Phys. Rev. C **54**, 1843 (1996).
[18] S. Karataglidis, P. J. Dortmans, K. Amos, and C. Bennhold, Phys. Rev. C **61**, 024319 (2000).
[19] Y. Suzuki, Nucl. Phys. **A528**, 395 (1991).
[20] K. Varga, Y. Suzuki, and Y. Ohbayasi, Phys. Rev. C **50**, 89 (1994).
[21] S. Funada, H. Kameyama, and Y. Sakuragi, Nucl. Phys. **A575**, 93 (1994).
[22] P. Navratil, W. E. Ormand, E. Caurier, and C. Bertulani, Lawrence Livemore National Laboratory, UCRL-PROC-211912 (2005).
[23] M. Milin *et al*., Nucl. Phys. **A730**, 285 (2004).
[24] O. R. Kakuee *et al*., Nucl. Phys. **A728**, 339 (2003).
[25] E. A. Benjamim *et al*., Phys. Lett. **B647**, 30 (2007).
[26] L. Borowska, K. Terenetsky, V. Verbitsky, and S. Fritzsche, Phys. Rev. C **76**, 034606 (2007).
[27] A. A. Korsheninnikov *et al*., Nucl. Phys. **A616**, 189 (1997).
[28] L. V. Chulkov *et al*., Phys. Rev. Lett. **79**, 201 (1997).
[29] A. N. Ostrowski, Nucl. Phys. **A701**, 19c (2002).
[30] T. Matsumoto, E. Hiyama, K. Ogata, Y Iseri, M. Kamimura, S. Chiba, and M. Yahiro, Phys. Rev. C **70**, 061601(R) (2004).
[31] A. M. Moro, K. Rusek, J. M. Arias, J. Gomez-Camacho, and M. Rodriguez-Gallardo, Phys. Rev. C **75**, 064607 (2007).
[32] M. Kamimura *et al*., Prog. Theor. Phys. Suppl. **89**, 1 (1986).
[33] M. Yahiro *et al*., Prog. Theor. Phys. Suppl. **89**, 32 (1986).
[34] G. R. Satchler, *Direct Nuclear Reactions* (Oxford University Press, Oxford, 1983).
[35] I. J. Thompson, Comput. Phys. Rep. **7**, 167 (1988).
[36] M. El-Azab Farid and M. A. Hassanain, Nucl. Phys. **A678**, 39 (2000).
[37] M. Karakoc and I. Boztosun, Phys. Rev. C **73**, 047601 (2006).
[38] M. Karakoc and I. Boztosun, Int. J. Mod. Phys. E **15**, 1317 (2006).
[39] R. Raabe *et al*., Phys. Rev. C **67**, 044602 (2003).
[40] H. T. Fortune and G. S. Stephans, Phys. Rev. C **25**, 1 (1982).
[41] D. R. Orber and O. E. Johnson, Phys. Rev. **170**, 924 (1968).
[42] D. E. Trcka, A. D. Frawley, K. W. Kemper, D. Robson, J. D. Fox, and E. G. Myers Phys. Rev. C **41**, 2134 (1990).